Intrinsically disordered coral acid-rich protein regulates growth of calcium carbonate phases through liquid-liquid phase separation

Barbara P. Klepka, Agnieszka Michaś, Tomasz Wojciechowski, and Anna Niedźwiecka

Laboratory of Biological Physics, Institute of Physics, Polish Academy of Sciences, Aleja Lotników 32/46, 02-668 Warsaw, Poland; annan@ifpan.edu.pl

Introduction

Biomineralization mechanisms described within the framework of non-classical crystallization (NCC) theory involving putative liquid precursors is attracting increasing attention[1]. Unlike the classical crystallization pathway, NCC assumes that crystal formation occurs through intermediate states such as prenucleation clusters, amorphous precursors, or the liquid phases, rather than through simple atom or ion attachment[2]. The sequential emergence of these states and/or their coexistence in equilibrium, along with their transformations dependent on thermodynamic conditions, is still a matter of debate. The putative pre-nucleation stage, PNCs, comprise 1-3 nm clusters of ions that are both thermodynamically stable and highly hydrated[3]. Another hypothesized transient state, amorphous calcium carbonate (ACC), has been found in living biomineralizing organism. These ACC entities were postulated to form within the tissue and subsequently attach to the skeleton's surface, where they eventually undergo crystallization to aragonite ($CaCO_3$ polymorph)[4]. The transient liquid phase is postulated to be formed in the presence of polymers and is referred to as polymer-induced liquid precursors (PILPs)[5]. There is, however, no direct evidence of PILPs involving proteins. On the contrary, it was speculated that PILPs are, in fact, assemblies of ACC clusters driven by polymers[6]. In the context of coral skeleton formation, these polymers could be appointed to *i.a.* coral acid-rich proteins (CARPs) secreted to the coral extracellular matrix. By far, only four CARPs have been cloned and partially characterized[7]. CARPs have low-complexity sequences enriched in disorder-promoting charged amino acid residues, such as Asp and Glu, typically for intrinsically disordered proteins (IDPs). IDPs exhibit high conformational flexibility, making them extremely sensitive to environmental conditions. Many IDPs can undergo liquid-liquid phase separation (LLPS)[8] and form liquid biomolecular condensates.

Here we report the properties of a fifth polyelectrolytic CARP – the aspartic and glutamic acid-rich protein (AGARP) from *Acropora millepora* coral[9], which is a model organism to study coral development and biocalcification. We provide experimental evidence that the highly charged AGARP with a net charge of -148 e per molecule and a linear charge density of -0.77 e/nm is an IDP that can strongly affect both the early stages of $CaCO_3$ nucleation and crystal growth. In particular, we introduce a new, potential, biologically relevant crystallization precursor – Protein-Calcium Liquid Condensate (PCLC) composed of CARPs and sequestered Ca^{2+} formed *via* LLPS in viscous, crowded environment mimicking coral extracellular skeletal organic matrix.

Aspartic and glutamic acid-rich protein (AGARP) is intrinsically disordered

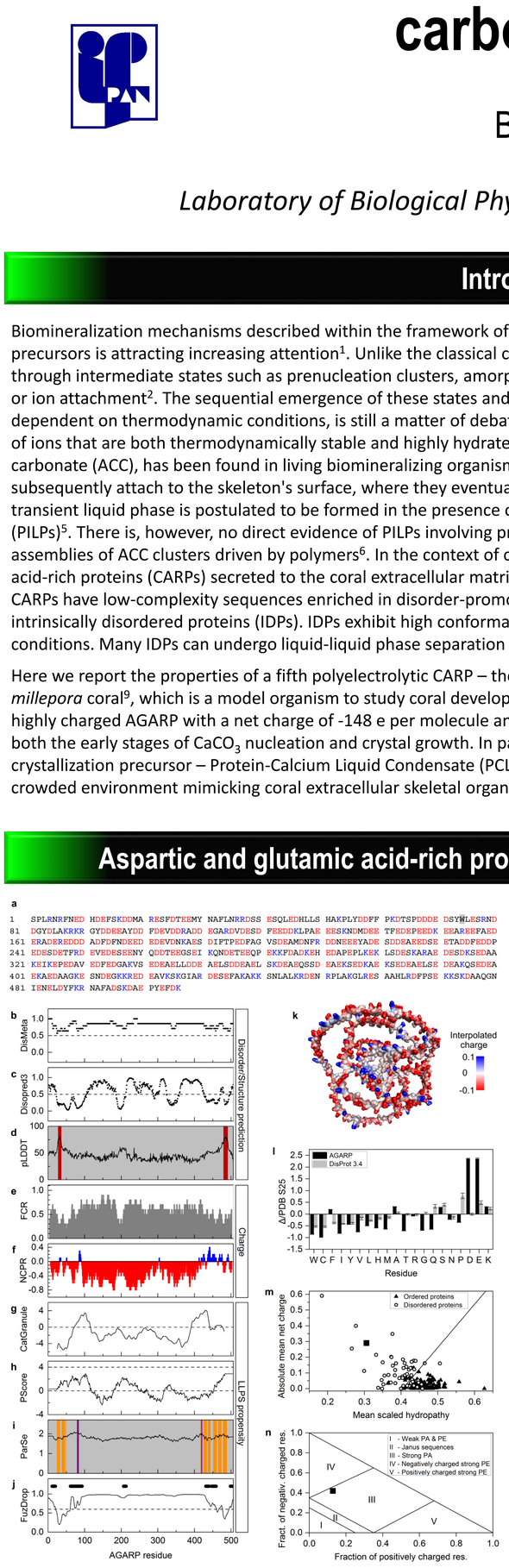

Figure 1. Predicted properties of AGARP.
(a) AGARP sequence without signal peptide with colored acidic (red) and basic (blue) residues and tryptophan highlighted in gray (Uniprot: B7W112). Bioinformatics analysis of AGARP: **(b,c)** disorder tendency, **(d)** secondary structure prediction, **(e,f)** charge distribution, **(g-j)** LLPS propensity, **(k)** putative conformation predicted by AlphaFold2 shown in the solvent-accessible surface representation and colored according to interpolated charge, **(l)** composition profile, **(m)** charge-hydropathy plot, and **(n)** Das-Pappu phase diagram. Dashed lines denote the thresholds of respective methods of prediction. Values exceeding the threshold indicate that a region is **(b,c)** disordered or **(g-j)** prone to LLPS. α-helices predicted with pLDDT ≥ 70 in **(d)** are marked dark red. Positive NCPR in **(f)** are marked dark blue and negative - dark red. In panel **(i)**, grey - regions intrinsically disordered but not prone to LLPS, orange - regions that can fold to a stable conformation, and violet - intrinsically disordered regions prone to undergo LLPS. Thick black lines in **(j)** mark aggregation hot-spots. Amino acids in **(l)** are ordered relative to the flexibility of the residue. In **(n)**, PA stands for polyampholytes and PE for polyelectrolytes.

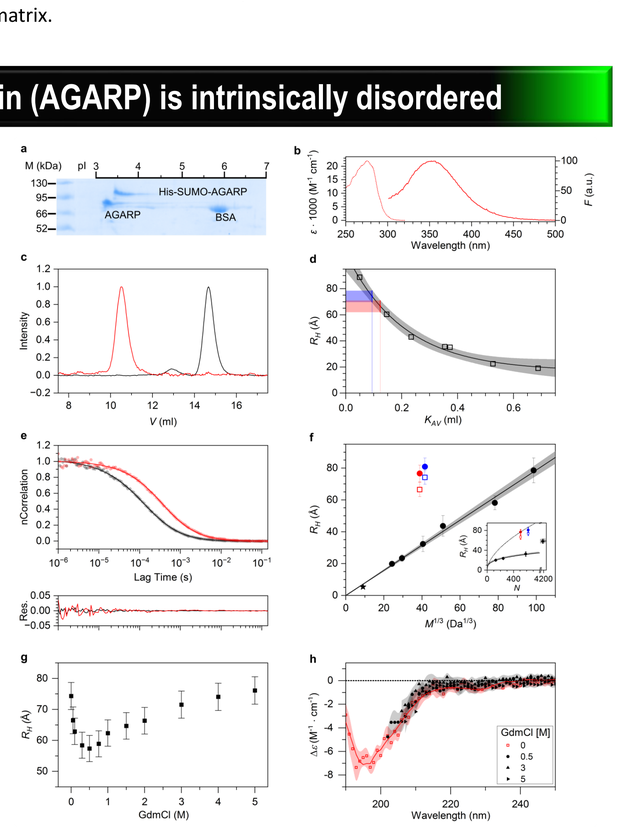

Figure 2. Experimentally determined properties of AGARP and His_6-SUMO-AGARP.
(a) 2D IEF SDS PAGE of AGARP and His_6-SUMO-AGARP. BSA as a mass and pI standard, **(b)** UV absorption (dotted line) and emission (solid line) spectrum of AGARP, **(c)** SEC profile of AGARP (red line) and HSA (black line), **(d)** Hydrodynamic radii of AGARP (red) and His_6-SUMO-AGARP (blue) from SEC at 10 °C with shaded errors. Exponential function (black line) fitted to data points for model folded protein (open black squares). **(e)** Example normalized FCS autocorrelation curves for AGARP (red) and HSA (black) (dots, experimental points; lines, fitted models of diffusion) (upper panel) with corresponding fitting residuals (bottom panel), **(f)** Dependence of R_H on $M^{1/3}$ determined by FCS for folded proteins (black circles), AGARP (red circle) and His_6-SUMO-AGARP (blue circle) at 25 °C and by SEC at 10 °C (hollow squares). Linear function fitted to the values for folded proteins and freely diffusing AF488 (black star) with 95% CI. (inset) R_H *vs.* number of protein residues, N; power function ($R_H = R_0N^{\nu}$) (solid black line) fitted to experimental points for folded proteins with 95% CI; dotted black line, power function for denatured proteins ($R_H = 2.21N^{0.57}$ Å [10]), **(g)** Changes of AGARP R_H with increasing concentration of GdmCl as determined by SEC at 10 °C, **(h)** CD spectra of AGARP in the presence of different concentrations of GdmCl at 10 °C. Points - averaged experimental data with shaded SD, solid line – BeStSel fit.

Liquid-liquid phase separation of AGARP triggered by Ca^{2+}

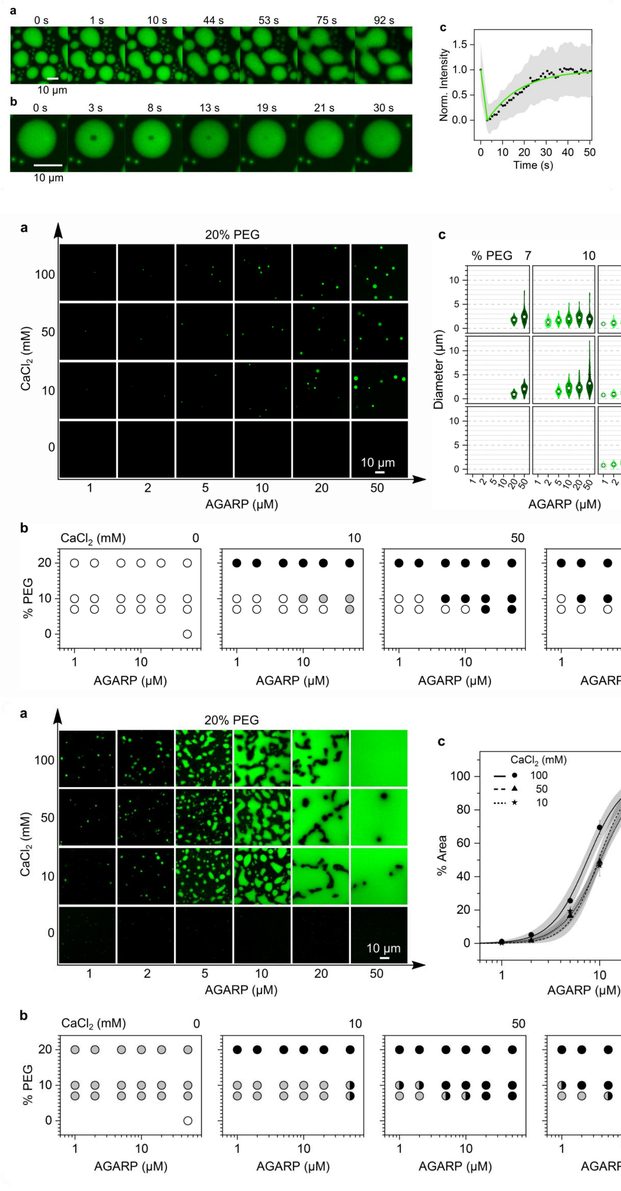

Figure 4. Liquid properties of the droplets formed after 5 min at 50 µM AGARP, 100 mM $CaCl_2$ and 10% PEG 4k.
(a) Fluorescence confocal microscopy images of coalescence of droplets; **(b)** Fluorescence recovery after photobleaching and **(c)** the corresponding FRAP curve. Shaded area, standard deviation of intensities; green line, one component exponential function fitted in FRAPAnalyzer 2.1.0.

Figure 5. Ca^{2+}-driven LLPS of AGARP observed 5 µm above the microscopic slide.
(a) Fluorescence confocal microscopy images of droplets formed in 20% PEG in the presence of varying concentrations of AGARP and $CaCl_2$. **(b)** Phase diagram of LLPS. Black, droplets; white, no droplets or aggregates; gray, aggregates. **(c)** Droplets diameter distribution. Increasing intensity of green colour denotes increasing concentration of AGARP in the sample.

Figure 6. Spinodal decomposition observed on the surface of the microscopic slide.
(a) Fluorescence confocal microscopy images of AGARP-rich phases formed in 20% PEG in the presence of varying concentrations of AGARP and $CaCl_2$. **(b)** Phase diagram for LLPS. Black, droplets or phases formed as a result of droplets coalescence; white, no droplets or aggregates; gray, aggregates. gray/black; both droplets and aggregates. **(c)** Percentage of area occupied by AGARP-rich liquid phase at 20% PEG 4k as a function of AGARP concentration. Hill function was fitted to experimental data points (lines with 95% CI).

AGARP induces nucleation, slows down growth, and rounds edges of $CaCO_3$ crystals

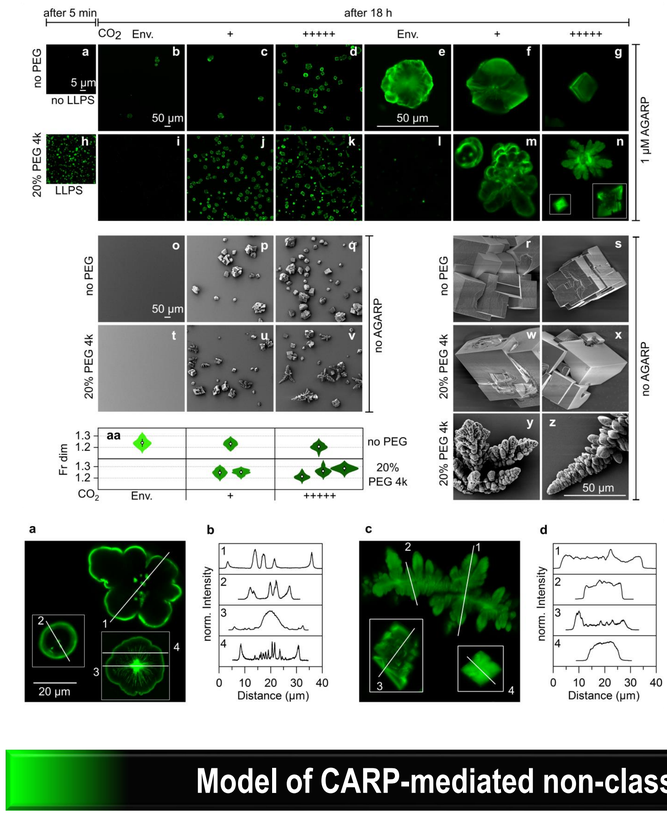

Figure 7. $CaCO_3$ phases and crystals grown in the presence and absence of AGARP with and without 20% PEG 4k after 18 h of crystallization at increasing concentrations of CO_2.
Fluorescence confocal microscopy images of **(a,h)** phases formed in the presence of AGARP at 1 µM prior to crystallization, **(b,c,d,i,j,k)** $CaCO_3$ phases formed at increasing concentrations of CO_2 in the presence of AGARP. SEM images in the absence of AGARP **(o,p,q,t,u,v)**. Characteristic phases grown under given conditions imaged by confocal microscopy **(e,f,g,l,m,n)** and SEM **(r,s,w,x,y,z)**. CO_2 conditions: Env. - environmental; + and +++++ - in the presence of 12.5 and 62.5 mg/cm³ $(NH_4)_2CO_3$, respectively. **(aa)** Fractal dimensions of the phases shown in panels **(e,f,g,m,n)** determined using ImageJ and FracLac. Hollow black circle, mean; black line, standard deviation.

Figure 8. AGARP distribution in $CaCO_3$ phases and crystals grown in the presence of AGARP at 1 µM, 20% PEG 4k after 18 h of crystallization.
Fluorescence confocal microscopy images of AGARP-containing $CaCO_3$ phases grown in the presence of **(a)** 12.5 mg/cm³ and **(c)** 62.5 mg/cm³ $(NH_4)_2CO_3$ as a source of CO_2, with white profile lines shown in **(b)** and **(d)**.

AGARP-driven formation of amorphous calcium carbonate (ACC)

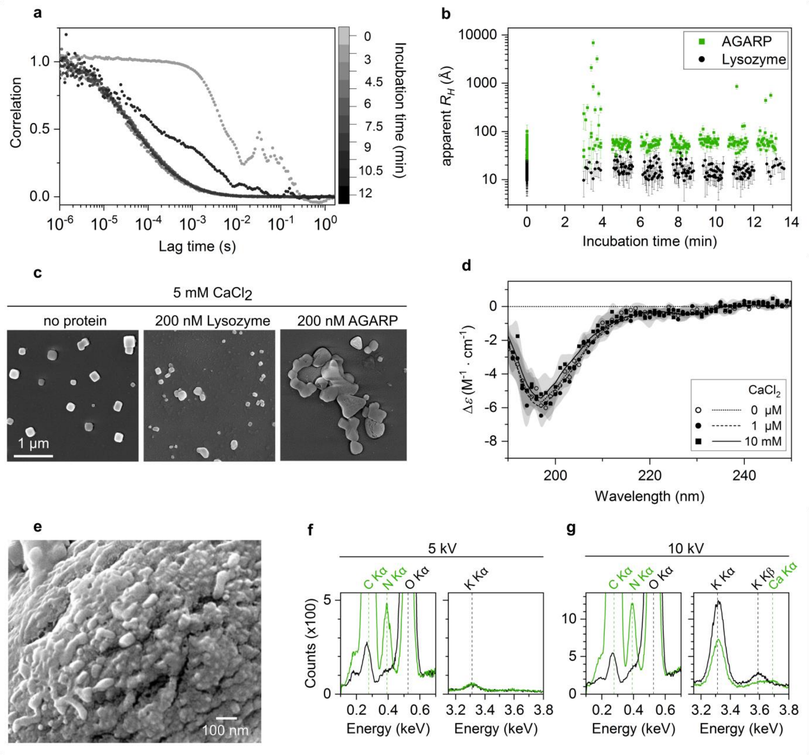

Figure 3. Interaction of AGARP with Ca^{2+} leads to aggregation and amorphous precipitation of $CaCO_3$.
(a) Normalized FCS autocorrelation curves obtained for 200 nM AGARP at subsequent time points after the addition of 5 mM $CaCl_2$. **(b)** Apparent R_H values from FCS of the species containing AGARP and lysozyme (control) shown as a function of incubation time with Ca^{2+}. **(c)** SEM images of the phases deposited on the glass slide after the FCS experiment. **(d)** Normalized circular dichroism spectra of AGARP in the absence and presence of $CaCl_2$. Points indicate averaged experimental data with SD marked as shade. Lines are fits performed by BeStSel. No secondary structures or conformational changes were detected. **(e)** SEM image of the fragment of the phase formed after the FCS experiment analyzed by EDS at 5 kV AV. **(f, g)** EDS spectra obtained at **(f)** 5 kV and **(g)** 10 kV accelerating voltage. Green spectrum, $CaCO_3$ phase containing AGARP; black spectrum, glass slide (control); dashed lines, K lines of the elements.

Model of CARP-mediated non-classical crystallization pathway

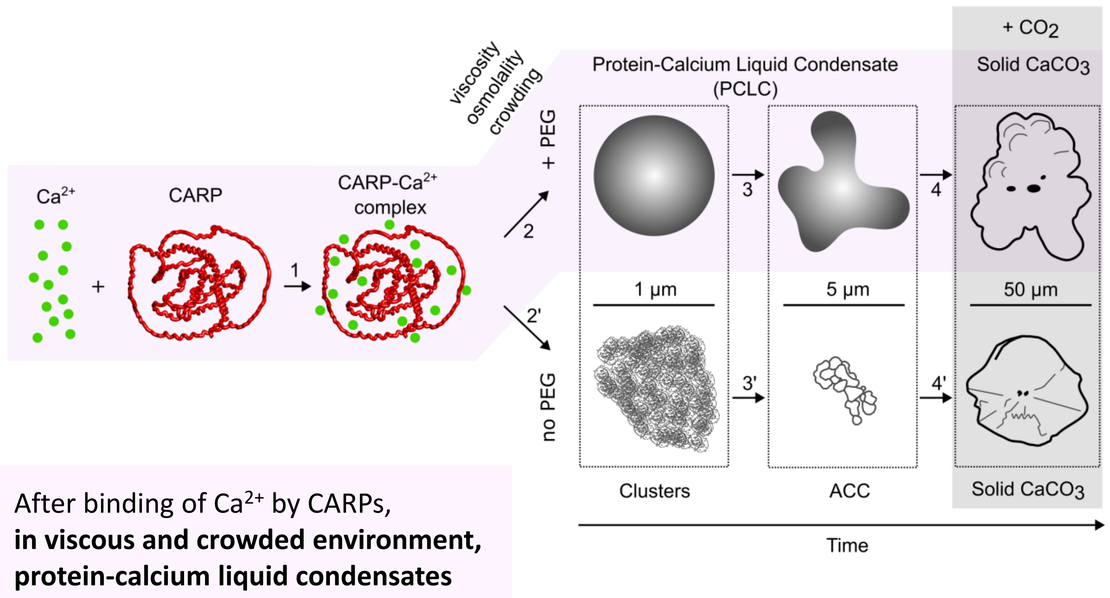

1. After binding of Ca^{2+} by CARPs,
2. **in viscous and crowded environment, protein-calcium liquid condensates (PCLCs) are formed *via* liquid-liquid phase separation.**
3. PCLCs coalesce forming higher-order liquid phases.
4. In the environment rich in CO_2, crystallization occurs based on PCLCs, and $CaCO_3$ crystals with well developed and rounded edges appear.

2'. Under less crowded/viscous conditions, CARP-Ca^{2+} complexes undergoes aggregation,
3'. followed by the transformation to amorphous calcium carbonate (ACC).
4'. Once ACC is exposed to CO_2, crystallization takes place, and $CaCO_3$ crystals with sharp edges are formed.

Acknowledgements:
Supported by NCN of Poland grant 2016/22/E/NZ1/00656 and NanoFun ERDF POIG.02.02.00-00-025.

References: [1] Avaro, J. T. *et al.*, **Angew Chem Int Ed**, 6155–6159, 2020. [2] Jehannin, M. *et al.*, **JACS**, 10120-10136, 2019. [3] Avaro, J. *et al.*, **JPCL**, 4517-4523, 2023. [4] Mass, T. *et al.*, **PNAS**, E7670-E7678, 2017. [5] Gower, L. B., Odom, D. J., **J Cryst Growth**, 719-734, 2000. [6] Xu, Y. *et al.*, **Nat Commun**, 2582, 2018. [7] Mass, T. *et al.*, **Curr Biol**, 1126-1131, 2013. [8] Alberti, S. *et al.*, **Cell**, 419-434, 2019. [9] Ramos-Silva, P. *et al.*, **Mol Biol Evol**, 2099-2112, 2013. [10] Wilkins, D. K. *et al.*, **Biochemistry**, 16424-16431, 1999.